J. Micromech. Microeng. **20** (2010) 015044 (12pp) doi:10.1088/0960-1317/20/1/015044

A full description of a scalable microfabrication process for arrayed electrowetting microprisms

L Hou, J Zhang, N Smith, J Yang and J Heikenfeld

Novel Devices Laboratory, Department of Electrical and Computer Engineering, University of Cincinnati, Cincinnati, OH 45221, USA

E-mail: heikenjc@ucmail.uc.edu

Received 14 September 2009, in final form 23 November 2009
Published 18 December 2009
Online at stacks.iop.org/JMM/20/015044

Abstract

Most electrowetting and liquid crystal optical devices are created by standard planar microfabrication. Arrayed electrowetting microprisms are a newer approach that offers unique performance, but which requires a challenging non-planar microfabrication process. This paper reviews a full description of a scalable fabrication process for an ~1500 element array of ~150 μm size electrowetting microprisms. The description includes creation of high aspect-ratio sidewalls, using a conventional i-line mask aligner to vertically pattern electrodes, conformal hydrophobic dielectric deposition, self-assembled and volume-controlled liquid dosing and module sealing. Also presented is a theoretical model which explores the resolution limits for vertically patterned electrodes. In addition to creating a first-generation fabrication process for arrayed electrowetting microprisms, this work may be further useful to investigators seeking methods of forming 3D arrayed electro-optic, electro-chemical or electro-mechanical devices.

(Some figures in this article are in colour only in the electronic version)

1. Introduction

Arrayed optical technologies have reached a remarkable state of maturity when considering the resolution of charge-coupled imaging devices and the scale of liquid crystal displays that are now manufactured at >100″ diagonals. There are enormous infrastructure and electronics supporting arrayed electro-optics. However, the electro-optic devices themselves are still far from satisfying the ultimate requirements for applications such as reflective displays [1] or large-aperture beam steering [2]. Electrowetting [3] offers multiple new approaches [4] that may supersede the optical performance of technologies such as liquid crystals. For example, electrowetting displays [5] can provide >55% reflectance, and a simple scalable fabrication process has been demonstrated [6]. Transmissive [7–9] or reflective [9] electrowetting microprisms may also offer record beam steering performance. However, unlike electrowetting displays, electrowetting microprisms require two to four times more electrodes per device, a 3D enclosure for liquids, conformal dielectric deposition and a high-index contrast between liquids. Large ~mm size electrowetting prisms have been fabricated using simple means [9], but fabricating arrays of microscale electrowetting prisms has not yet been demonstrated.

Reported herein is a full description of a first-generation fabrication process for an ~1500-element array of ~150 μm size electrowetting microprisms. The fabrication process uses dominantly scalable tools found in most university facilities and liquid-crystal display fabrication lines. The description includes creation of high-aspect-ratio sidewalls, using a conventional i-line mask aligner to vertically pattern electrodes, conformal hydrophobic dielectric deposition, self-assembled and volume-controlled liquid dosing, and module sealing. Also presented is a theoretical model which explores the resolution limits for vertically patterned electrodes. Electrowetting microprisms might find applications in holographic displays [10], laser radar [11], solar lighting and agile imaging, to name a few. However none of these applications are attainable without creation of a scalable microfabrication process. Therefore this work is an important

 © 2010 IOP Publishing Ltd Printed in the UK

first step toward practical applications of arrayed microprisms. In addition to creating a first-generation fabrication process for the microprisms, this work may be further useful to investigators seeking methods of forming arrayed and highly non-planar electro-optic, electro-chemical or electro-mechanical devices.

2. Overview of electrowetting microprisms

For steering light, a transmissive architecture is generally preferred as it reduces the optical system footprint. Substantial progress is being made in transmissive steering technologies [2], but no technology has demonstrated the multi-wavelength and polarization-independent beam deflection that is achieved with a classical glass prism. An electrowetting microprism attempts to replace the refractive properties of a glass/air prism refraction with that of a high-index-oil/low-index-aqueous meniscus refraction. The prisms provide control over the prism apex angle through electrowetting [3], which is an electromechanical effect [12] that can modulate the aqueous/oil contact angle on a hydrophobic dielectric. By applying a voltage between the aqueous phase and an electrode beneath the hydrophobic dielectric the contact angle can be varied from Young's contact angle ($\theta_Y \sim 160$–180°) to an electrowetted contact angle ($\theta_V \sim 30$–60°). Contact angle versus voltage is predicted by the electrowetting equation:

$$\cos\theta_V = \frac{\gamma_{od} - \gamma_{ad}}{\gamma_{ao}} + \frac{CV^2}{2\gamma_{ao}}, \qquad (1)$$

where C is capacitance per unit area of the hydrophobic dielectric and γ is the interfacial surface tension between the aqueous liquid (a), oil (o) and the dielectric (d) [3]. Typically an ~1–3 μm Parylene C and fluoropolymer stack are used to create the hydrophobic dielectric, but as predicted by equation (1), the lower C results in a higher operation voltage of ~30–120 V. For lower voltage operation, 100 nm Al_2O_3 and 50 nm Asahi Cytop can be implemented to achieve <15 V operation [13].

In a basic electrowetting microprism, the contact angle change at two opposite sidewalls is used to tilt the aqueous/oil meniscus. As long as the voltages are selected such that contact angles are complimentary, the meniscus is held flat and a variable prism is created [7, 14]. An even more powerful embodiment is to confine the liquids inside square cubes with four independent electrowetting sidewalls. As shown in figure 1, a prism can thereby be tilted over two dimensions [9]. Because the oil is of higher refractive index than the aqueous liquid, light propagating through the prism is deflected toward the side of the prism with thicker oil, and therefore substantially avoids the sidewalls. As shown in figure 2(a), single prism arrays can theoretically be sandwiched together to form a double prism array. As a result, the beam deflection can be quite large (figure 2(b)), especially when the refractive index of the oil is increased to >1.6 [15].

The wide-angle beam steering performance of electrowetting microprisms [16] could prove to be highly attractive for a variety of applications. However, many applications require a large optical aperture (>10s of cm). A single prism alone

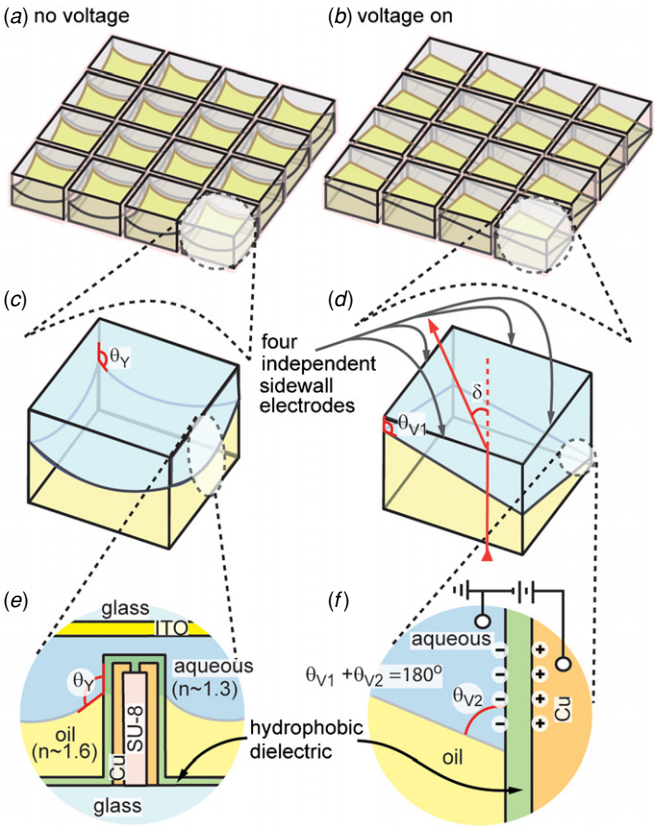


Figure 1. Diagrams (a, b) of electrowetting microprism operation without and with voltage; (c, d) a zoom in of individual prism operation; (e, f) a further zoom in detailing the role of electrowetting in control of the oil/aqueous meniscus.

cannot satisfy this requirement, because even if the aqueous and oil liquids are density matched, gravity and vibration will cause the meniscus to sag for individual prisms greater than a centimeter in size. Therefore the only viable option for these applications is to microfabricate micro-prisms in large arrays.

In the subsequent sections of this paper we will review the process steps for creating a first-generation electrowetting microprism array. A photograph of a prototype resulting from this fabrication process is shown in figure 3(a). As shown in figure 3(b), an optical demonstration was performed by imaging the prism array through a microscope. A blue and a yellow LED top-side illuminated the array from opposite off-axis angles. The prism array was switched between the OFF state with a curved meniscus and the ON state with a repeated triangular profile. For the triangular profile, the LED light Fresnel reflected at the oil/aqueous meniscus. This demonstration vehicle consisted of an array of 1500 prisms; each prism is created with a square cube of dimensions 150 μm × 150 μm × 112 μm. The 150 μm size was chosen because it is at the scale where the prisms would begin to satisfy the requirements for laser radar or holographic displays. Such requirements include scalable fabrication using conventional LCD-style tools and fast switching speed (smaller size results in faster speed [17]). In addition, a phased-array profile is often desired, which requires the prisms to be small such that they can be accurately controlled by arrays of

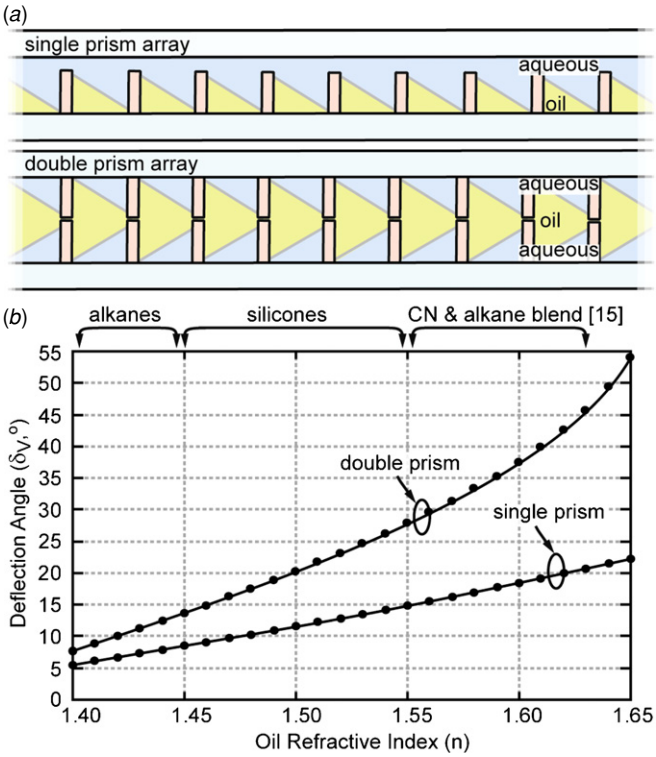


Figure 2. (*a*) Diagrams showing implementation of single and double electrowetting prism arrays for beam steering and (*b*) calculations of potential beam steering performance for the arrays versus refractive index (contact angle is 43°).

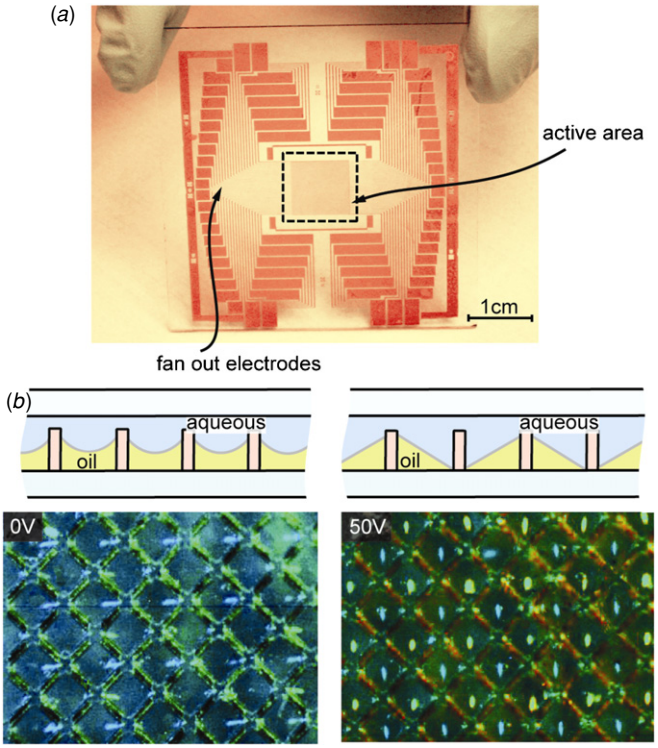


Figure 3. (*a*) Photograph of electrowetting microprism array prototype including the electrode fan-out and (*b*) diagrams and microscope photographs of a simple demonstration of the prism array under two-axis LED illumination.

active-matrix transistors. With an example prism array now demonstrated, our discussion turns toward the main topic of this paper: a description of the fabrication process for arrayed electrowetting microprisms.

3. Arrayed electrowetting microprism fabrication and discussion

The fabrication process contains five major steps: sidewall fabrication (figure 4(*a*)), 3D electrode patterning (figures 4(*b*)–(*e*)), hydrophobic dielectric coating (figure 4(*f*)), liquid dosing (figure 4(*g*)) and sealing (figure 4(*h*)). Fabrication starts with leveling negative photoresist on top of glass, followed by UV (365 nm) imaging to form an array of square enclosures, herein referred to as cells. The sidewall photolithography process uses standard negative-acting photoresists, but as will be seen, the prisms impart several non-standard requirements on the photoresists. Following the sidewall fabrication, metal electrodes are coated and wet-etch patterned across all the sidewall structures. This 3D electrodes patterning is the most challenging step because it requires not only conformal photoresist coating but also angled UV exposure and electrode etch chemistry that is compatible with the specialized conformal photoresist. After the photoresist is patterned, the electrode wet etch is performed. Because the goal of this work is merely to demonstrate a workable first-generation fabrication process, as shown in figures 3(*b*) and 4(*d*) and (*e*), only two-electrode control of prism arrays was implemented. However, the process described herein is fully extendable to patterning four sidewall electrodes per prism. Next a hydrophobic dielectric is coated, with special consideration that it must be deposited at relatively lower temperature and in a highly conformal manner. At this point, the solid prism 'cell' is finished and ready for self-assembled liquid dosing.

However, unlike previous self-assembled liquid dosing for electrowetting displays [1, 18] both the oil and aqueous liquid must occupy the cells, each at ∼50% of the prism volume. Lastly, the device is UV epoxy sealed with an upper plate coated with a transparent electrode. The sealing must be performed while the prism array is immersed in aqueous solution. After sealing, the prism array is ready for wiring and electro-optical testing.

Each process will now be detailed including all critical considerations, challenge level and alternate techniques where applicable. Some aspects of prism array fabrication were found to be more challenging than initially expected. However, research was continued until a first-generation process was developed that can likely be implemented in any lab with standard microfabrication capability. All fabrication was performed on 2 × 2″ square wafers cut by PG&O Inc. from larger sheets of display-standard aluminosilicate glass (Corning Inc.).

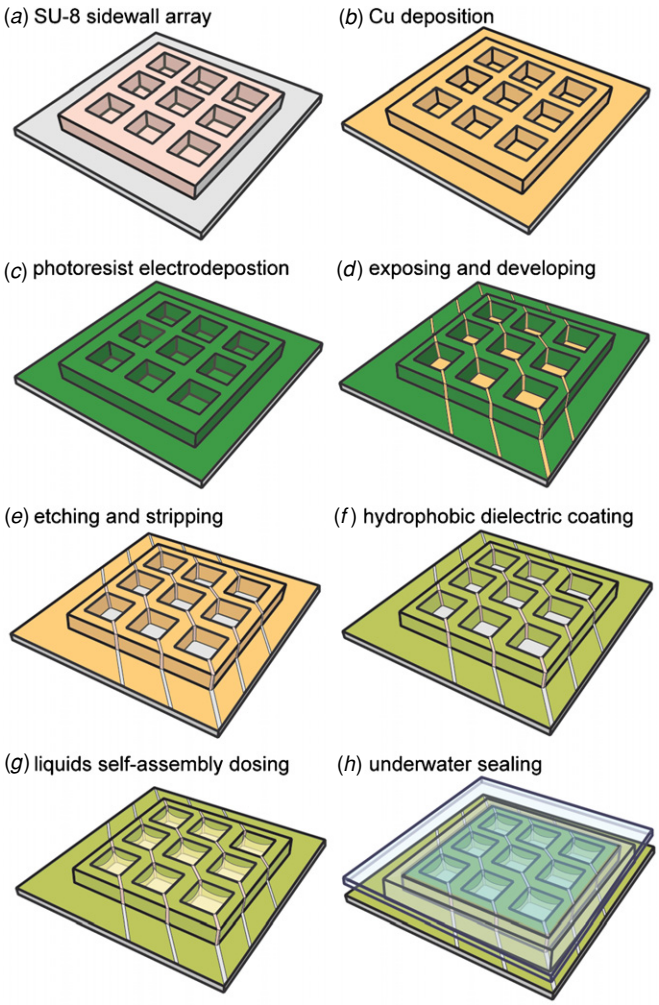


Figure 4. Diagram of the prism array fabrication process: (*a*) sidewall fabrication; (*b*) metal film deposition; (*c*) electrodeposited conformal photoresist; (*d*) angled photoresist exposing and developing; (*e*) metal etching and photoresist stripping; (*f*) hydrophobic dielectric coating; (*g*) self-assembled liquid-dosing; (*h*) underwater sealing.

3.1. Sidewall fabrication

The prism sidewalls must satisfy a challenging set of requirements. The sidewalls must be economical to process, chemically and physically stable throughout prism fabrication and operation, smooth to prevent electrical high-field points or contact angle hysteresis, and be able to eventually achieve high fill factor (∼10:1 or greater aspect ratio). It was quickly determined that negative acting and permanent photoresists are the technology of choice over alternates such as polymer microreplication or prolonged plasma etching.

Three exemplary negative acting photoresists were explored in detail: SU-8 (MicroChem), KMPR (MicroChem) and PerMX dry film (Dupont). SU-8 and KMPR are both i-line sensitive (365 nm) epoxy-based photoresists. PerMX is a newly developed dry film negative photoresist that is sensitive from 200 nm to 450 nm with a peak absorption at 365 nm, and in our opinion is remarkable in terms of process speed and repeatability. All of these three products are highly UV transparent, thus enabling exposure of thick films (10s to 100s of μm). Although the final dimension of the prisms fabricated herein will be >100 μm, the above photoresists are readily scalable to only a few 10s of μm dimension. A comparison of the process for all three resists is provided in table 1. With respect to applying the photoresist to the substrate, PerMX excels above both SU-8 and KMPR because it is simply hot-roll laminated as dry film. Not only does this eliminate the long soft-bake times needed to remove the solvent from thick liquid photoresists but the films are much more uniform in height (no edge beads). Also, PerMX films do not require a precise leveling of the substrate, which is mandatory for thick liquid resists during the soft-bake cycle. PerMX exhibited <2 μm variation in thickness whereas the spin-coated thick layer of SU-8 and KMPR normally exhibited around a 10 μm thickness variation from the edge to the center.

Adhesion to the substrate must also be very good because the photoresist films were thick and therefore have greater strain during thermal cycling. KMPR and PerMX showed very good adhesion after hard bake, while the patterned cells of SU-8 suffered a major peeling off problem from bare glass, even after hard bake. To improve SU-8 adhesion, an ∼1 μm seed layer of SU-8 2002 was first deposited and cured over the entire glass wafer. As a result the effective contact area between the SU-8 and substrate was far more than that of just the sidewall area. Chemical or mechanical roughening of the glass substrate was also seen to improve SU-8 adhesion, even at roughness levels that were not visible (optically scattering).

Next, the photoresist coatings were transferred to an EVG420 i-line mask-aligner. Regarding exposure, KMPR was the most sensitive to UV exposure dose, and PerMX was the most forgiving. If under-exposed, all three photoresists exhibited poorer adhesion. If over-exposed, all the three photoresists produced sidewalls that were not perfectly vertical (sloped). Propylene glycol monomethyl ether acetate (PGMEA) solvent was utilized to develop all three photoresists. Spray developing was found to be necessary for clean development of KMPR samples, and was found to be helpful for speeding up the SU-8 development. PerMX developed remarkably fast and developed cleanly even without liquid agitation. The exposing and developing parameters are also provided in table 1.

Lastly, a hard bake was implemented to remove any remaining solvent and to complete the chemical cross-linking. SU-8 and KMPR were baked at 180 °C, while PerMX can be baked at 120 °C or less. In some cases, a higher temperature hard-bake is preferred if higher temperature dielectric deposition or fluoropolymer annealing will be implemented later. It is better to cause any thermal deformation of the sidewalls before subsequent thin film coatings are added. The SU-8 and KMPR sidewalls were measured with an AFM, and roughness values (*Ra*) were found to be 0.14 nm and 0.21 nm, respectively.

At this point, DuPont PerMX seemed to be an exemplary choice for prism sidewall fabrication. Before concluding on a preferred photoresist, completed sidewall cells were soaked in 1-chloronaphthalene, an oil that is compatible with electrowetting and has a high refractive index of $n \sim 1.63$ [15]. Not all prism arrays will necessarily require this oil, as there

Table 1. Comparison of processing steps for SU-8, KMPR and PerMX photoresists for prism sidewall fabrication.

	Coating method/ parameter	Glass adhesion	Soft-bake (hotplate)	Expose @365 nm (EVG 420 aligner)	Post-bake (hotplate)	Develop (PGMEA)	Hard bake (oven)
SU-8 2100	Spin-coating 15 s @ 500 rpm and 114 rpm/min 40 s @ 2200 rpm and 344 rpm/min	Poor, need seed layer	65 °C ~3.5 h [19] leveled surface	36 s @10 mW cm^{-2}	5 min, 65 °C 10 min, 95 °C	10–15 min stirring	180 °C 60 min
KMPR 1050	Spin-coating 10 s @ 500 rpm and 114 rpm/min 40 s @ 1000 rpm and 344 rpm/min	Good	100 °C 30 min leveled surface	140 s @10 mW cm^{-2}	10 min, 100 °C	5 min spray @ 40 psi	180 °C 60 min
PerMX 3050	40 psi, 80 °C hot roll 10 min cool before second lamination Western Magnum 12″ Laminator	Good	None required	72 s @10 mW cm^{-2}	10 min, 100 °C	5 min soak	120 °C 30 min

are a variety of silicone oil blends that can provide $n \sim 1.55$. However, 1-chloronaphthalene is a very strong solvent and would give some insight into the chemical stability of the sidewall structures. As shown in figure 5(*a*), SU-8 and KMPR were unchanged after 12 h of soaking in 1-chloronaphthalene, but PerMX was found to swell and deform in less than 30 min.

After completing the above tests, SU-8 was chosen as the sidewall fabrication material because it was believed that it would provide superior resistance to solvents and electrowetting liquids. Angled and cross-section SEM photographs of the SU-8 sidewalls are shown in figure 5(*b*). KMPR may be stable in solvent, but the fact that it can be developed in an aqueous alkaline solution caused concern over its long-term stability in water. It is conceivable that SU-8 might be able to be implemented in a laminated dry-film format similar to PerMX, but unfortunately no manufacturer currently provides such a product.

3.2. Electrode patterning over the 3D sidewall structure

The next task after sidewall fabrication is electrode patterning on the sidewalls, which is the most challenging part of the entire prism fabrication process. The process includes metal deposition, conformal photoresist coating, exposure, develop, metal etch and photoresist stripping. The choice of electrode material and etchant is dependent on the photoresist coating process and will not be detailed until the end of this section.

3.2.1. Options explored for conformal photoresists. Three methods were initially explored to achieve a conformal photoresist coating over the 3D sidewalls: modified spin-coating, ultrasonic spray coating and electrodeposited photoresist.

Modified spin-coating uses a conventional spin coater, but the substrate was inverted during the coating process to reduce excess accumulation in the deeper topography of the surface [20]. Several diluted solutions of AZ4620 were tested, and indeed the inverted substrate outperformed the standard upright substrate. However, the process was highly unrepeatable, particularly for large area patterns. Furthermore, inside the prism cells the photoresist was unacceptably thick at corner features.

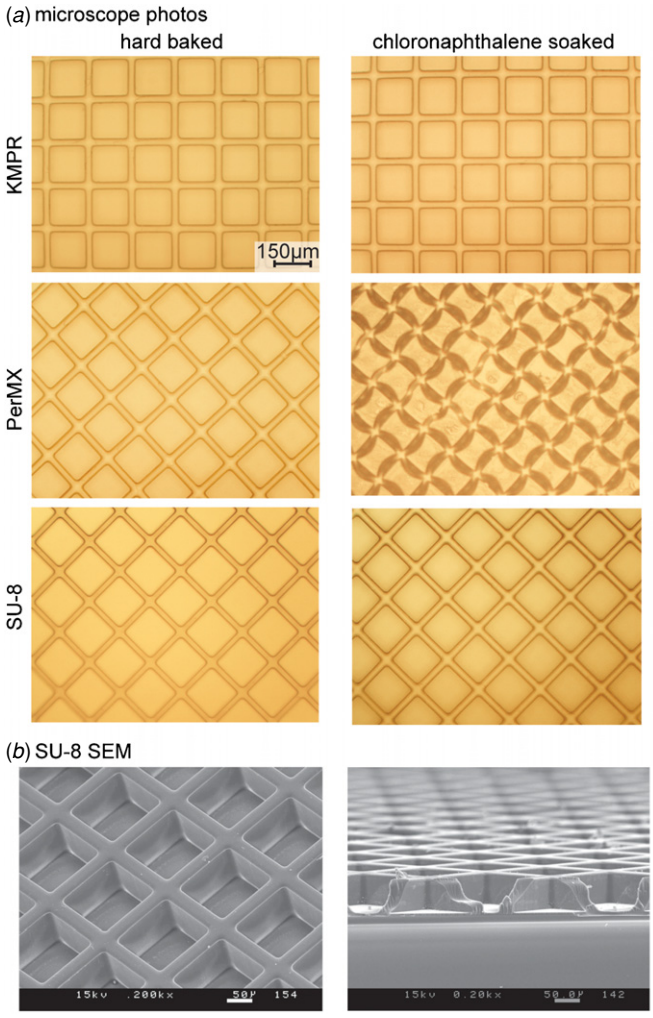


Figure 5. (*a*) Microscope photographs of 1-chloronaphthalene resistance tests for SU-8, KMPR and PerMX sidewalls; (*b*) scanning electron microscope photographs for the SU-8 sidewalls.

Next, ultrasonic spray coating was attempted. Ultrasonic spray coating employs a high frequency (~100 kHz) ultrasonic nozzle that changes a flow of dilute photoresist solution (<20 Cst) into an ultra-fine mist of ~20 μm droplets, which will become smaller when reaching the substrate due to solvent

evaporation [21]. At such small droplet size, the photoresist literally appears like smoke as it leaves the nozzle. To direct this ultra-fine mist to the substrate, compressed nitrogen is ejected near the nozzle tip. For the work reported herein, a Sonotek accuMist^{TM} nozzle (120 kHz) was mounted at a 30° angle to the substrate. During spraying the substrate was rotated at 7.5 rpm. Using a stepper motor, the nozzle was also scanned across the substrate diameter with a 0.9448, 1.0986, 1.3184, 1.6479, 2.1973, 6.5918, 4.3945, 2.1973, 4.3945, 6.5918, 2.1973, 1.6479, 1.3184, 1.0986, 0.9448 rpm speed profile. The best coating results were achieved with 1 part AZ4620 diluted with 0.5 parts PGMEA and 3 parts MEK. The PGMEA solvent served the purpose of slowing the drying time of the mist; else one would simply deposit micro-beads of dried photoresist [21]. After repeated experimentation and optimization, a process was found where the droplets were dry enough to stick to the sidewalls instead of running down the sidewalls as liquid. However, there was always a distribution of droplets that were so dry that they bounced off sidewalls, and because of gravity, accumulated as a thicker coating on horizontal surfaces. This problem was partially resolved by implementing the entire setup as described above, but in a manner in which the entire substrate was rotating in the vertical plane. After switching to vertical substrate orientation, the process was found to be successful on a few samples, but the results were far from repeatable from run to run. Particularly challenging was the unavoidable thinner coating of photoresist at corners on top of the prism sidewalls, and much thicker coating at bottom corners. The thicker coating at the bottom corners requires larger exposing dose, while the thinner coating at the top sharp corners would not survive the develop step or would not properly act as an etching mask for the electrode. It was determined that ultrasonic photoresist coating, while possibly attractive for coating electrically insulating surfaces, was entirely a too slow and difficult process to be considered for electrowetting microprism arrays.

Next, electrodeposited photoresist was explored. Unlike ultrasonic photoresist coating, electrodeposited photoresist requires deposition on an electrically conductive surface. This is not an issue for prism arrays, as the whole goal of this photoresist coating is to act as an etching mask for an underlying electrode coating. Electrodeposited photoresist is typically an aqueous emulsion containing ion-charged organic photosensitive micelles. Such micelles are normally 50–200 nm and stable in aqueous suspension due to surface charge [22]. The deposition is performed by migrating the micelles along the electric field generated with a high voltage (∼150 V) applied between the metalized sample substrate and a reference electrode. For lab scale experiments, a simple and economical setup was constructed (figures 6(*a*) and (*b*)). Although there are commercially available equipments for electrodeposition of photoresists, the setup described herein can successfully be implemented in any microfabrication facility.

3.2.2. Optimization of electrodeposited photoresist coating. To begin the process, InterVia 3D-P (Rohm & Haas) emulsion was first diluted with DI water from 20% to 10% solid

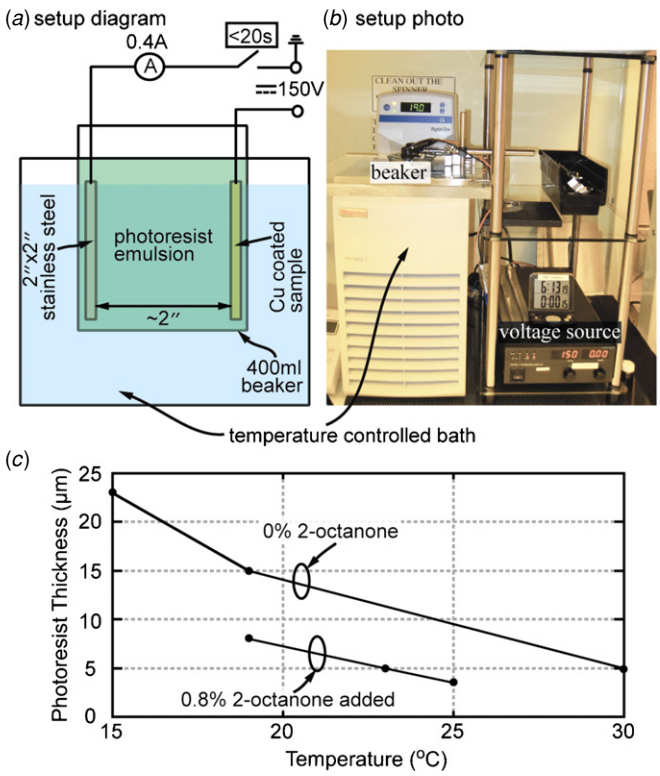


Figure 6. Photoresist deposition setup and thickness control: (*a*) and (*b*) schematic drawing and photograph of equipment set-up; (*c*) thickness control of photoresist deposition by controlling deposition temperature and solvent content.

(includes photosensitive resin and other function parts, e.g. dye) concentration in a 400 ml beaker by magnetic stirring for 15 min. If placed in a properly sealed container and stored in a 5–10 °C refrigerator, the diluted emulsion was found to be stable for greater than 1 month. The beaker of diluted photoresist emulsion was also found to be reusable for ∼20 electrodepositions.

The beaker of diluted photoresist emulsion was placed in a temperature-controlled water bath. The 2 × 2″ prism array including an electrode coating over entire substrate and prisms was inserted into the emulsion as the anode. A 2 × 2″ stainless steel plate was then inserted into the emulsion as the cathode, with a uniform 2″ separation between the anode and cathode. A constant 150 V dc voltage was then applied, and the negatively charged micelles migrated toward and conformally coated the metalized prism array surface. The coating was highly conformal because the photoresist is electrically insulating and the electrodeposition process is locally self-terminated once the photoresist reaches a desired thickness. Process completion was witnessed externally as the current dropped from a peak value of 0.4 A to zero in a period of only ∼10–20 s. Next the sample was removed from the emulsion and immediately rinsed with DI water to remove any emulsion remaining inside the prism cells. The sample was thoroughly dried with a nitrogen gun, and then soft-baked at 100 °C for 8 min to further coalesce the micelles and smooth the photoresist coating. The process of electrodepositing photoresist was found to be very fast and

repeatable, and therefore the electrodeposited photoresist was explored in greater detail than either the inverted spin-coating or ultrasonic spray coating.

Contrary to what one might expect, the thickness of electrodeposited photoresist is not practically controllable with voltage because the process is current terminated once a conformal and defect-free coating is achieved. As shown in figure 6(*c*), the thickness can be substantially controlled by varying the emulsion temperature or the concentration of 2-octanone in photoresist emulsion [23]. At higher temperature, the micelles more readily flow and form a complete insulating coating, thus terminating the coating process at a thickness as small as ∼5 μm. 2-octanone can be added slowly into photoresist emulsion with a stirring bar (>1 h). The 2-octanone is one of the solvent components of photoresist emulsion and can reduce the coating thickness by making a finer spreading of photoresist micelles. After completing optimization, including other factors to be discussed in the next section, 19 °C and 0.8 wt% addition of 2-octanone was considered optimal and resulted in ∼8 μm photoresist thickness.

Three different sputter-deposited electrode materials were investigated: In_2O_3:SnO_2 (ITO), Al and Cu. All of these electrode materials were implemented at ∼150 nm thickness and satisfy the requirements for electrical operation of the electrowetting microprisms, but their compatibility with the photoresist electrodeposition was found to vary widely. It was found that aluminum was always partly etched during electrodeposition because of the basic nature of the emulsion (pH ∼ 11). No etching was observed for ITO or for Cu. Cu exhibited a long-term adhesion problem on SU-8 and therefore a 10 nm Ti coating was evaporated onto the SU-8 sidewalls before the Cu metal was deposited.

The electrode material must also promote complete wetting of the emulsion inside the prism cells. The contact angles of the emulsion on the metals were measured to be 72° for ITO, 75° for Al and 61° for Cu. Even though these contact angles satisfy the condition for capillary wetting, it was still difficult to dislodge a single large air bubble inside each prism cell. The effect of an air bubble during photoresist coating is visually apparent in SEM photographs of figure 7(*c*). As a first attempt to resolve this problem, the substrates were placed in vacuum, and the vacuum was replaced with DI water. The substrate with DI water filled inside prism cells was then placed in the bath of photoresist emulsion. However, as visually apparent in figure 7(*a*), even placing the sample in the emulsion for >10 min, a thinner photoresist coating was achieved anywhere that DI existed. Instead of investigating this phenomenon further, an alternate process was explored. The electrode materials were plasma treated in low power (100 W) oxygen plasma for 20 s and then immediately placed into the photoresist emulsion. Plasma treatment increased the surface energy of the substrate, and as shown in figures 7(*b*) and (*c*) a conformal and defect-free photoresist coating was achieved.

3.2.3. Angled exposure of the conformal photoresist. Intervia 3D-P photoresist is i-line (365 nm) sensitive and

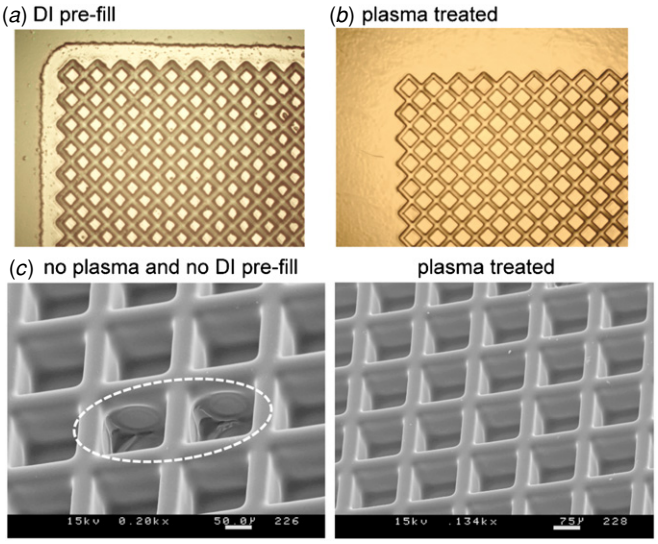


Figure 7. Optimization of the electrodeposited photoresist process includes attempts to improve wetting of the photoresist emulsion by (*a*) water pre-filling under vacuum and (*b*) oxygen plasma surface modification; SEM photographs are provided in (*c*) which compares the photoresist coating with and without the occurrence of air bubble trapping inside the prism cells.

works in positive mode, which is preferred because positive photoresists can typically resolve finer features than negative photoresists. The photosensitive material in Intervia 3D-P is diazonaphthoquinone, which will form a ketene with UV exposure, and then react with water to form indene carboxylic acid [22]. Because of the role of water in the photoresist chemistry, it was found that the photoresist processing results varied wildly with humidity changes in our lab. Therefore, humidity control was installed such that both the soft-bake and exposure were always performed in 40% relative humidity.

Conventional lithography is adequate for exposure of horizontal photoresist coatings or those on slightly sloped surfaces [24]. However, the prism sidewalls are vertical, and require UV light that is incident at an angle to the substrate. Therefore, as shown in figure 8, two different types of exposures were carried out on the same photoresist film. A traditional UV exposure with a first mask was used to expose photoresist at the bottom of the prism cell. Exposing the resist at the bottom of the cell is needed because an optical aperture must be etched in the electrode. Also, this traditional UV exposure step was used to pattern the electrode fan-outs for interconnect (figure 3(*a*)).

After traditional exposure, a glass prism with a refractive index of 1.536 at 365 nm and an apex angle of 45° was used to tilt the collimated UV beam by $\alpha \sim 27.7°$. The glass prism was aligned such that the tilted beam of UV was directed toward and thus exposed one vertical corner surface of the prism sidewalls. Using a simple line mask, if two-electrode control is desired then two prism exposures are required (one for each opposite corner). If four-electrode control is implemented, then four such exposures are required. For the first-generation process implemented herein, a triangular prism profile was demonstrated (figure 3(*c*)) because it requires only two angled exposures. However, four prism exposures were also

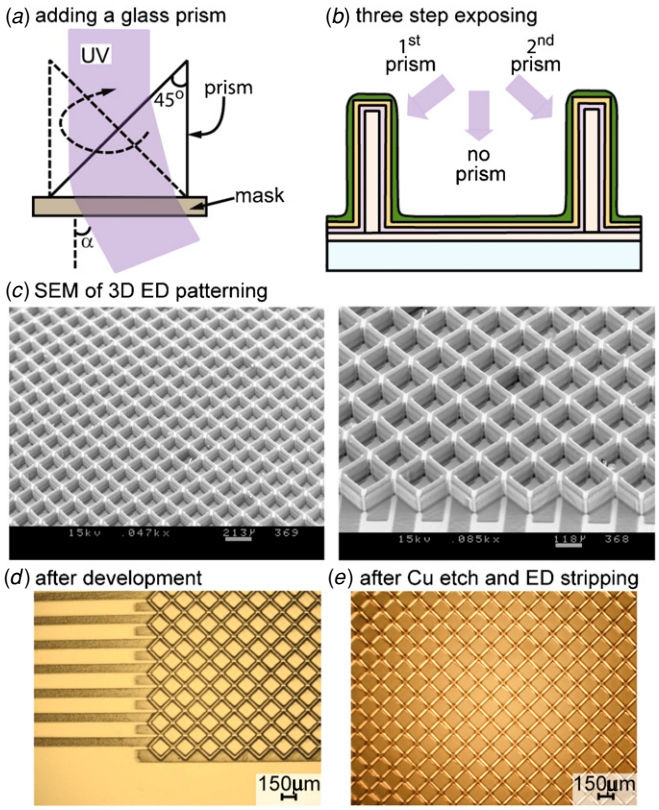


Figure 8. Diagrams of (*a*) adding a large glass prism to the mask aligner for angled exposure and (*b*) the two angled and one traditional exposure steps needed to pattern the photoresist. Two SEM photographs (*c*) are shown after exposure and development of the photoresist. Microscope photographs are shown (*d*) after development (*e*) and after etching of the Cu electrodes and photoresist stripping.

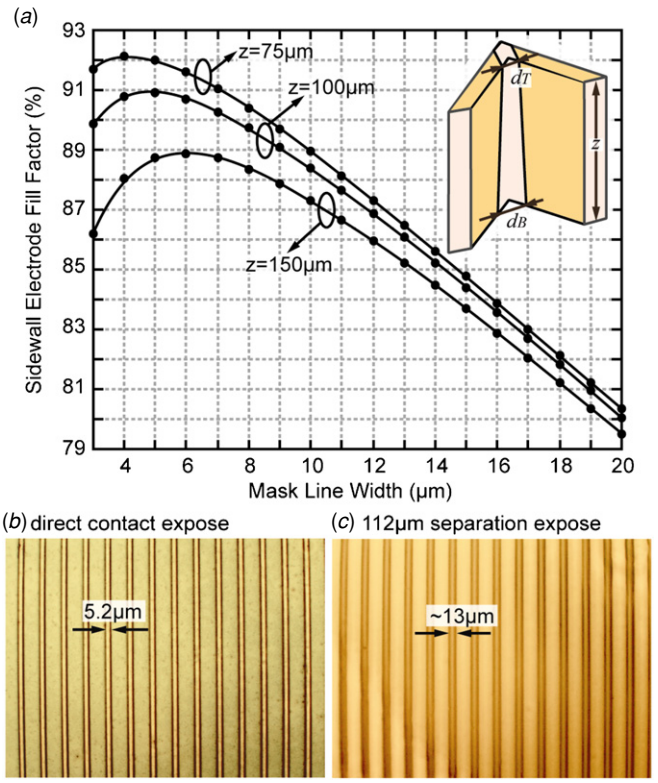


Figure 9. Line-width resolution for angled exposing method: (*a*) theoretical calculation of sidewall electrode fill factor; (*b*) line width resolution test for direct contact exposing; (*c*) line width resolution test for 112 μm separation between the mask and photoresist.

validated. In some ways, copper is an ideal electrode for angled exposure because it exhibits a reflectance of only 33% at 365 nm, and therefore reduces unwanted UV reflection and subsequent misplaced UV exposure. The angled exposures required longer time than traditional exposure because of several factors: (1) Fresnel reflection from the prism itself (~4.5% per surface); (2) at the 27.7° incidence angle the UV intensity was reduced by 47.5%; and (3) the photoresist coating was thicker in the sidewall corners because the resist had a concave geometry. After optimization, repeatable exposure results were achieved with an underlying Cu electrode, 40 s for traditional exposure (10 mW cm^{-2}) and 120 s for each angled exposure (~3 mW cm^{-2}). After development, the patterning results are shown in the photograph of figure 8(*d*). The development process itself requires multiple constraints and will be detailed in a later section. Before discussing photoresist development and electrode etching, the resolution limits of the photoresist patterning will be presented in greater detail.

Optimized exposure of the prisms requires careful consideration of the mask line-width, because the mask cannot be in immediate proximity with all the photoresist layers. As shown in the inset diagram of figure 9(*a*), some unavoidable line broadening will occur further away from the mask due to diffraction. A narrower mask line-width will reduce the exposed resist width at the top of the prism (d_T) but at some point, continued narrowing of mask line-width will cause diffraction and actual widening of the exposed photoresist width at the bottom of the prism (d_B). Increased separation between adjacent sidewall electrodes will then locally induce a meniscus that is not flat and degrade the prism optical performance. The non-flat meniscus occurs due to Young's angle [25] in the non-electrode regions and the electrowetted contact angle in the adjacent electrode regimes. Therefore, a smallest possible line-width must be achieved at both d_T and d_B.

Before even considering the effects of diffraction, one should ensure that the photoresist coating is able to replicate the width of the UV beam. A 5 μm thick Intervia 3DP photoresist layer was therefore exposed with a 5 μm line-width mask for the case of direct contact. As shown in figure 9(*b*), it was confirmed that the Intervia 3DP is capable of achieving 1:1 aspect ratio for direct contact exposure. Herein, ~8 μm of photoresist was found to give the most reliable coating and electrode etching results. Therefore if a 1:1 aspect ratio limit is assumed, then the minimum line-width is currently ~8 μm, even without the effects of diffraction.

Now discussed are the effects of diffraction on the exposure resolution. The intensity distribution of UV light after passing through the mask can be calculated according to single slit diffraction theory. For the prism geometry herein, the condition for Fraunhoffer (far-field) diffraction

is only slightly satisfied as the mask distance from the bottom of the prism (∼112 μm) is close to the square of the minimum mask line-width (5 μm) divided by the wavelength (0.365 μm). For larger mask line-widths, Fresnel (near-field) diffraction begins to factor in. Numerical simulation is not trivial for this problem, and practical material considerations and process variation must be taken into consideration. Therefore, ultimately it is recommended that one simply perform exposure and development tests of several mask line-widths lesser and greater than 5 μm. Such optimization was not performed herein, but theoretical and experimental insights into electrode fill factor will now be discussed.

Assuming Fraunhoffer diffraction only, a model was created that assumed the photoresist would not be exposed after an angle at which the central diffraction peak falls to 30% of the original UV intensity ($\theta_{30\%}$). The achievable photoresist line-width at the bottom of the prism cavity (d_B) can therefore be calculated according to

$$d_B = d_T + \frac{2z \tan \theta_{30\%}}{\cos\alpha}, \tag{2}$$

where additional terms are the UV incident angle α diagramed in figure 8(*a*), and the height of the prism cells z diagramed in the inset drawing of figure 9(*a*). As a reminder, d_T is equal to the mask line-width because the mask will contact the top of the prism sidewalls. The electrode fill factor (*FF*), for the case of four independent sidewall electrodes, can then be calculated as

$$FF = 1 - \frac{\sqrt{2(d_T + d_B)}}{(a + b)}, \tag{3}$$

where a and b are the prism cell width and length (∼150 μm each). As shown in the plot of figure 9(*a*), the fill factor increases linearly with decreasing mask line-width, until the onset of substantial broadening of the central diffraction peak. Again, the results plotted in figure 9(*a*) do not take into account near-field diffraction for the mask line-width >3 μm. However, this is not of practical concern because diffraction-limited line-width does not occur until ∼5 μm line-width, which is in the Fraunhoffer regime. Herein, the prism cell height is ∼112 μm, and from equations (2) and (3) the maximum electrode fill factor is theoretically ∼90% for the case of four independent sidewall electrodes. It was found that experimental results agree with theory, as the results pictured in figure 9(*c*) show d_B ∼13 μm and therefore a fill factor of ∼91.5%.

3.2.4. Photoresist developing and electrode etching. Like conventional positive photoresist, post-bake is not necessary, so after exposure the sample was ready for developing. The sample was then placed in a beaker of commercially available Intervia 3DP developer, which is mainly tetramethylammonium hydroxide. An alternate developer is a 5% sodium carbonate solution [23]. Both of these developer solutions etch Al, providing another reason why Cu is preferred over Al electrodes. The development was performed at room temperature and requires ∼2–3 min for tetramethylammonium hydroxide and ∼10–15 min for sodium carbonate. Generally, sodium carbonate was preferred as it provided more repeatable results, less undercut and better resistance to delamination of the photoresist film. After development, a reflow bake at 110 °C was also experimented with and found to help smooth the profile of the photoresist etching mask. However, in the end, the reflow bake was not implemented because it made photoresist stripping from the 3D prism structures very difficult.

For etching the electrode materials a variety of wet etchants were explored. Many etchants, including phosphoric:nitric:acetic, hydrochloric acid and hydrofluoric acid either attacked or caused delamination of the Intervia 3DP photoresist. For Cu electrodes, a highly repeatable etchant was ferric chloride [23]. The ferric chloride solution was 1 wt% and required ∼4 min etching time at room temperature. A solution of 0.5 wt% hydrofluoric acid was then used to further etch the Ti adhesion layer beneath the Cu electrode. For Al electrodes, the best approach for etching was to develop and etch the photoresist and Al using the same solution of sodium carbonate. However, Al etching was less reliable than that of Cu and therefore the Cu electrode was again preferred over Al. For ITO, etching was achieved in ∼5 min with a mix composed of 3 wt% oxalic and 1 wt% tartaric acid in DI [26]. Despite good etching results, ITO was not preferred over Cu because of increased cracking and less repeatable electrodeposition of photoresist. In summary, Cu was the preferred electrode material.

After etching, the photoresist was stripped using an acetone rinse. The recommended Intervia 3D-P stripper, and heated (55 °C) NMP (*N*-methylpyrrolidone) were also tried but all of them tended to leave a white residue after development. To prepare the samples for the next step of dielectric coating, the samples were therefore further cleaned by an oxygen plasma ash for 5 min at 100 W. The photographs of the patterned Cu electrode are shown in figure 8(*e*).

3.3. Hydrophobic dielectric coating

To generate the electromechanical force that allows reversible and reliable electrowetting, a dielectric coating is required between the aqueous solution and the sidewall electrodes. The dielectric surface must also be hydrophobic to promote a large Young's angle and minimum contact angle hysteresis. Therefore, a thin top-coating of fluoropolymer is often added. There are numerous dielectric issues to be considered, including the relationship between dielectric failure and size of the molecules in the liquid [13]. Instead of reviewing all such properties we will herein review only those unique to prism array fabrication. Because the prism array is constructed of a highly non-planar surface supported by polymer (SU-8), a low temperature (<180 °C) and conformal dielectric deposition process is required. Example processes therefore include plasma-enhanced chemical vapor-deposition of materials such as SiOCH, atomic-layer deposition of Al_2O_3, and organic Parylene C or Parylene HT coating. Room-temperature Parylene C deposition was chosen for the prism arrays discussed herein because it is the simplest to implement of all these processes.

In order to coat the Cu electrodes with Parylene C, the prism arrays were placed inside a PDS 2010 Lab coater system

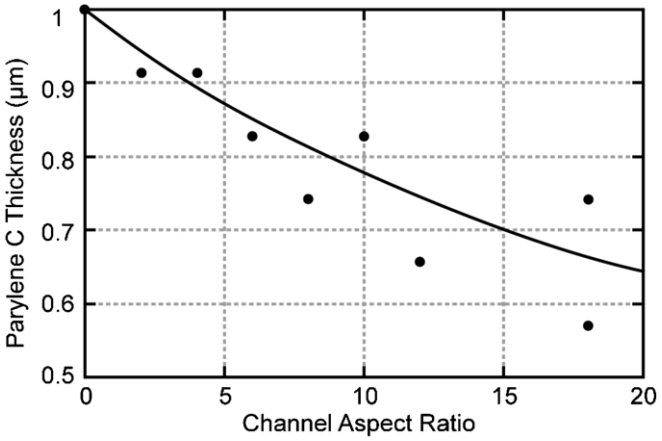


Figure 10. Conformality test of Parylene C dielectric coating on high aspect ratio channels.

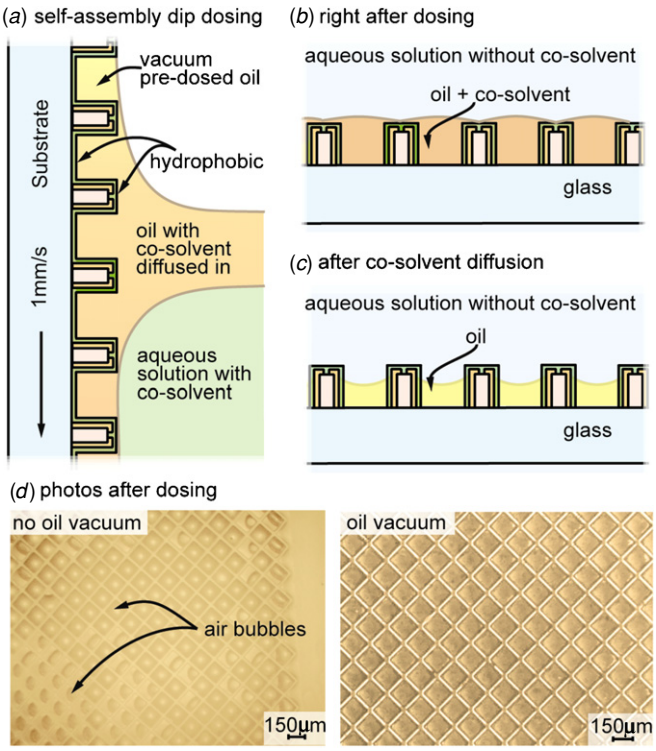


Figure 11. Volume-controlled self-assembly oil dosing process: (*a*–*c*) diagrams of the dip dosing process with co-solvent extraction and (*d*) photographs of dosed arrays without and with vacuum pre-dosing of oil into the prism cells.

for conformal deposition of an ∼5 μm film. The deposition process involves dimer vaporization, vapor pyrolysis, followed by room-temperature monomer deposition and polymerization on the substrate surface at ∼0.1 Torr. Generally, the dielectric coating thickness at the top of the prism sidewalls should be equal to the coating thickness at the bottom of the prism sidewalls. Substantial variation in thickness would cause a non-flat meniscus due to variation in dielectric capacitance (an electrowetted contact angle that varies across the sidewall). To mitigate concern over dielectric thickness variation, Parylene C coating was performed on a long channel that was 50 μm high and the decrease in Parylene C thickness recorded as a function of depth into the channel.

As shown in figure 10, the Parylene C thickness does exhibit substantial variation. If Parylene C is utilized it is therefore not recommended to exceed a 1:1 aspect ratio for the prism cell height/width. To provide the dielectric surface with proper hydrophobicity, a solution of 1 wt% fluoropolymer (Cytonix Fluoropel 1601 V) was dip-coated at ∼1 cm s^{-1} onto the prism array. After dip-coating, the sample was air dried for 20 min and then cured at 120 °C for 30 min in an oven. It is not possible to obtain a highly uniform fluoropolymer coating thickness by dip-coating the 3D prism array structure. Therefore, the fluoropolymer thickness was kept at <80 nm to minimize variation in the series capacitance for the dielectric stack of Parylene/fluoropolymer. It should be noted that the need for the fluoropolymer can be eliminated with use of oils having low interfacial surface tension with the parylene [27].

3.4. Self-assembled oil dosing

After hydrophobic dielectric coating, the prism array was ready for liquid dosing. If the liquid dosing is to be a scalable process then ink-jet or other serial dosing methods are not desired. Scalable self-assembly processes have been demonstrated for dosing colored-oil or pigment dispersions into electrowetting displays [1, 18]. Neither process is appropriate for prism arrays because the oil and aqueous liquids should each only occupy ∼50% of the volume inside each prism cell. Therefore, a modified self-assembly process was developed for the prism arrays, and for lens arrays reported elsewhere [28]. For simplicity, tetradecane oil was used, but a variety of other silicone and aromatic oils can be designed into the general self-assembly process. To begin, the substrate was vacuum dosed with oil. As shown in figure 11(*d*), even though the oil surface tension is low enough to allow wetting into the individual prism cells, the aspect ratio of the cells is high enough to cause air-bubble entrapment. For vacuum dosing the sample was vacuumed at 2.54 Torr while being immersed in oil for >30 min.

After vacuum dosing of oil into the prism cells, the substrate was then lowered vertically at ∼1 mm s^{-1} into a 2 mm thick oil film floating on aqueous solution (figure 11(*b*)). Both the oil film and the aqueous solution contain a co-solvent of PGMEA. The PGMEA was added such that at equilibrium, the oil phase will contain ∼50% PGMEA. After the substrate was fully dip-coated, it was then placed in a Petri dish at the bottom of the dip-coating tank and transferred to a new aqueous bath that contains no PGMEA. While in the new aqueous bath, the PGMEA diffuses out of the oil and the oil volume reduces to ∼50% filling of the prism cells. The aqueous bath was refreshed at least once. Otherwise, even a few % of PGMEA left in the oil will degrade the electrowetting response. The aqueous bath may contain surfactants, glycols, salts or other components that modify the oil/water surface tension, the allowable temperature range or the electrical conductivity of the aqueous solution, respectively [13].

3.5. Underwater sealing

Before removing the prism array from the DI water bath, a glass top plate and a surrounding spacer layer were sealed onto the array with UV epoxy (Loctite 350). The glass plate can be coated with a transparent electrode that allows electrical contact to the aqueous solution, or a metal pin may be inserted through the spacer layer. The UV epoxy does not make a strong bond with the fluoropolymer coating on the prism array substrate. Therefore, it is recommended to oxygen plasma treat the fluoropolymer surface outside the prism array. This completes the prism array fabrication process, and operational testing can now be performed (figure 3).

4. Summary and future work

Electrowetting microprisms may find applications in laser radar, holographic displays, solar lighting and agile imaging, to name a few. It is likely that none of these applications are attainable without creation of a scalable microfabrication process. We have presented a scalable first-generation fabrication process for an ∼1500-element array of ∼150 μm size electrowetting microprisms. The description includes creation of 5:1 aspect ratio sidewalls of negative acting photoresist, using a conventional i-line mask aligner to create 3D electrodes over vertical sidewalls with 90% fill factor, conformal hydrophobic dielectric deposition, self-assembled and volume-controlled oil-dosing and module sealing. We have also explored the theoretical limits for 3D electrode patterning. The processes created herein demonstrates feasibility of scalable fabrication for electrowetting microprisms and may be further useful to investigators seeking methods of forming 3D arrayed electro-optic, electro-chemical or electro-mechanical devices.

Because of material process variation across a substrate, it is generally difficult to create large arrays of devices with identical optical response. Therefore, a single voltage source controlling a line of prisms across the entire substrate is unlikely to be viable. Instead, we postulate that the prism array could be integrated on an active-matrix array of thin-film transistors [29]. Material process over small distances is likely uniform, and thin-film transistor control is not likely needed for every individual sidewall. Rather, a subset of prisms, such as a 25 × 25 sub-array of prisms, might be controlled using four thin-film transistors. A reduced number of thin-film transistors will help improve the optical transmission of the prism array device. Integration with thin-film transistors would be achieved likely with an electrically insulating SU-8 film that is patterned with electrode vias, followed by fabrication and integration of the prisms on top of that film.

After locally programmable voltage control is implemented, the prism array can then be tuned for optimal optical performance and validated using Shack–Hartmann or other optical measurement tools. It should also be noted that the material set implemented herein was mainly that which was convenient in order to complete a first-generation fabrication process. Higher performance electrowetting dielectrics and high index oils are known in the electrowetting community and could be adapted to the prism arrays in future work. Also, for maximum electrical reliability, it is recommended that the use of water be eliminated and replaced with other polar liquid such as glycols. This has been shown to improve electrical reliability [13] and will likely benefit the effort to make the arrays even larger and working with lower operating voltages (<15 V).

Acknowledgments

This work was supported, in part, by an NSF CAREER Award, no 0640964; by SeeReal Technologies (Dresden); and by an AFOSR Young Investigator Award, no 06NE223. In particular, the authors would like to thank Stephan Reichelt of SeeReal for creating the initial interest in a scalable prism array fabrication process. The authors would also like to thank Hagen Stolle, Bo Kroll, Gerald Fütterer and Hagen Sahm for their valuable inputs and continuous encouragement during this project.

References

[1] Heikenfeld J, Zhou K, Kreit E, Raj B, Yang S, Sun B, Milarcik A, Clapp L and Schwartz R 2009 Electrofluidic displays using Young–Laplace transposition of brilliant pigment dispersions *Nature Photon.* **3** 292–6
[2] McManamon P F 2006 Agile nonmechanical beam steering *Opt. Photon. News* **17** 24–9
[3] Mugele F and Baret J 2005 Electrowetting: from basics to applications *J. Phys.: Condens. Matter.* **17** R705–74
[4] Heikenfeld J, Smith N, Dhindsa M, Zhou K, Kilaru M, Hou L, Zhang J, Kreit E and Raj B 2009 Recent progress in arrayed electrowetting optics *Opt. Photon. News* **20** 21–6
[5] Hayes R A and Feenstra B J 2003 Video-speed electronic paper based on electrowetting *Nature* **425** 383–5
[6] Zhou K, Heikenfeld J, Dean K A, Howard E M and Johnson M R 2009 A full description of a simple and scalable fabrication process for electrowetting displays *J. Micromech. Microeng.* **19** 065029
[7] Smith N R, Abeysinghe D C, Haus J W and Heikenfeld J 2006 Agile wide-angle beam steering with electrowetting microprisms *Opt. Express* **14** 6557–63
[8] Kuiper S, Van De Walle G F A, Wolterink E M, Mertens M and Feenstra B J 2006 Apparatus for forming variable fluid meniscus configurations *US patent* No US 2006/0079728A1
[9] Hou L, Smith N R and Heikenfeld J 2007 Electrowetting manipulation of any optical film *Appl. Phys. Lett.* **90** 251114–3
[10] Reichelt S, Sahm H, Leister N and Schwerdtner A 2008 Capabilities of diffractive optical elements for real-time holographic displays *Proc. SPIE* **6912** 69120P
[11] McManamon P, Watson E, Bos P, Heikenfeld J, Serati S and Huikei X 2009 A review of phased array steering for narrow-band electro-optical system *IEEE Proc.* **97** 1078–96
[12] Jones T B 2005 An electromechanical interpretation of electrowetting *J. Micromech. Microeng.* **15** 1184–87
[13] Raj B, Dhindsa M, Smith N R, Laughlin R and Heikenfeld J 2009 Ion and liquid dependent dielectric failure in electrowetting systems *Langmuir* **25** 12387–92
[14] Kuiper S, Hendriks B H, Huijbregts L J, Hirschberg A M, Renders C A and Van As M A 2004 Variable-focus liquid lens for portable applications *Proc. SPIE* **5523** 100–9

[15] Zhang J, Meter D V, Hou L, Smith N, Yang J, Stalcup A, Laughlin R and Heikenfeld J 2009 Preparation and analysis of 1-chloronaphthalene for highly refractive electrowetting optics *Langmuir* **25** 10413–16
[16] Han W, Haus J W, McManamon P, Heikenfeld J, Smith N and Yang J 2009 Transmissive beam steering through electrowetting microprism arrays *Opt. Commun.* at press
[17] Smith N R, Hou L, Zhang J and Heikenfeld J 2008 Experimental validation of >1 kHz electrowetting modulation *UGIM 17th Biennial* pp 11–4
[18] Sun B, Zhou K, Lao Y, Heikenfeld J and Cheng W 2007 Scalable fabrication of electrowetting displays with self-assembled oil dosing *Appl. Phys. Lett.* **91** 011106–3
[19] Anhoj T A, Jorgensen A M, Zauner D A and Hubner J 2006 The effect of soft bake temperature on the polymerization of SU-8 photoresist *J. Micromech. Microeng.* **16** 1819–24
[20] Kutchoukov V G, Mollinger J R and Bossche A 2000 New photoresist coating method for 3-D structured wafers *Sensors Actuators* A **85** 377–83
[21] Pham N P, Burghartz J N and Sarro P M 2005 Spray coating of photoresist for pattern transfer on high topography surfaces *J. Micromech. Microeng.* **15** 691–7
[22] Hertlein W G, Törnkvist K and Smith K 2001 ED photo resist technology becomes a manufacturing process *Circuit World* **27** 6–15
[23] Schnupp R, Baumgärtner R, Kühnhold R and Ryssel H 2000 Electrodeposition of photoresist: optimization of deposition conditions, investigation of lithographic processes and chemical resistance *Sensors Actuators* A **85** 310–5
[24] Sharma V, Suriadi A B, Berauer F and Mittelstadt L S 2003 AlCu pattern generation on 3D structured wafer using multi level exposure method on electrodeposited polymer material *Mater. Res. Soc. Symp. Proc.* **766** E5.4.1–6
[25] Berthier J 2008 *Microdrops and Digital Microfluidics* (Norwich, NY: William Andrew Publishing)
[26] Tsai T and Wu Y 2006 Organic acid mixing to improve ITO film etching in flat panel display manufacturing *J. Electrochem. Soc.* **153** C86–90
[27] Maillard M, Legrand J and Berge B 2009 Two liquids wetting and low hysteresis electrowetting on dielectric applications *Langmuir* **25** 6162–7
[28] Smith N R, Hou L, Zhang J and Heikenfeld J 2009 Fabrication and demonstration of electrowetting liquid lens arrays *IEEE J. Disp. Tech.* **5** 411–3
[29] Feenstra B J, Hayes R A, Camps I G J, Dijk R V, Hage L M, Biggelaar T J P and Baken J M E 2004 1-in. Active matrix addressed electrowetting displays *Proc. Int. Disp. Workshops* p 1717